SHG Characterization of Different Polar Materials Obtained by in Situ Photopolymerization

C. Artal, M. B. Ros,* and J. L. Serrano

Química Orgánica, Facultad de Ciencias, ICMA, Universidad de Zaragoza, CSIC, 50009 Zaragoza, Spain

N. Pereda, J. Etxebarría, and C. L. Folcia

Física de la Materia Condensada, Facultad de Ciencias, Universidad del Pais Vasco, 48080 Bilbao, Spain

J. Ortega

Física Aplicada II, Facultad de Ciencias, Universidad del Pais Vasco, 48080 Bilbao, Spain

Received November 9, 2000; Revised Manuscript Received February 26, 2001

ABSTRACT: The structural, thermal, and nonlinear optic (NLO) characterization of different polar materials is reported. These materials, which range from side-chain polymers to anisotropic networks and gels, were prepared by in situ photopolymerization of their precursors in the ferroelectric SmC* liquid crystal phase. The influence of the structure, the percentage of cross-linker, and the degree of mobility of a common NLO-phore on the second harmonic generation (SHG) activity have been considered with the aim of analyzing the most suitable approach for practical applications. Slight improvements in the SHG d_{ij} coefficients of these polymeric materials compared to their parent low molecular mass starting compounds have been observed. However, from these studies, it can be stated that side-chain polymers and low cross-linking polymers are the most interesting materials from the point of view of both the NLO-activity and the ease of synthesis. These two types of materials provide stable room temperature thin films displaying SHG and electrooptic (EO) responses without the application of a poling field.

Introduction

The idea of using light for transporting and processing information has become reality since the discovery and the generalized use of lasers. However, progress in photonic technologies makes it necessary to develop new optical materials and, in particular, compounds with nonlinear optical (NLO) properties.

As a result of their high nonlinear polarizabilty at both molecular and bulk levels, this type of material gives rise to a wide range of NLO effects.[1] The so-called second order NLO phenomena are the most broadly studied and, of these phenomena, second harmonic generation (SHG) and linear electrooptic (EO) effect (Pockels effect) have attracted much attention due to their application in different lightwave circuit technologies.

For many reasons, organic materials occupy their own unique place in the search for new possibilities for NLO properties,[2] despite the fact that a common problem with many organic materials is their low degree of polar order, which is often not stable for prolonged periods of time. In 1991 Walba et al.[3] clearly proved that ferroelectric liquid crystals (FLCs) are a suitable subject for study in this field. FLCs are materials with thermodynamically stable polar order, a situation in contrast to that in conventional polymers. In addition, they can be easily integrated with semiconductors to produce optical quality devices and, therefore, they offer good prospects for use as ultrafast EO modulators.

Since then, several attempts to improve the nonlinear responses of FLCs have been reported, either involving the design of new FLC−NLO-phores or trying to control the molecular mobility in the noncentrosymmetric SmC* phase. The initial studies were focused on the design of low molar mass compounds,[3−6] although different alternatives in the fields of oligomers[7] and polymers[8−10] have afforded some of the most interesting results.

On the basis of the good NLO-phore structure of the compound **W314** reported by Walba et al.,[3] different high molar mass materials have been prepared (see Figure 1). We have determined the NLO activity of a wide range of polymeric materials: side-chain polymers (**P/mW314**), cross-linked copolymers (**P/mW314-A*n***, **P/mW314-B*n***, and **P/mW314-C*n***), gels (**G/W314-B*n***) (where ***n*** represents for the percentage of cross-linking agent) and anisotropic networks (**N/dxW314**). These materials offer different degrees of molecular mobility and have allowed us to propose the most suitable approach for practical applications as well as to study other structural aspects, such as the nature and percentage of cross-linking on the modulation of the properties.

In this paper, we report the preparation, characterization, and SHG measurement of these new materials. The Pockels effects of these systems have been reported elsewhere.[11] All of the materials were prepared by in situ photopolymerization of the corresponding low molar mass compounds in the FLC phase. This method was first reported in relation to FLC−NLO properties by Trollsås et al.[9,10]

To prepare the polymeric materials, different chiral compounds such as the monoacrylate **mW314** and the diacrylates **d10W314** and **d12W314** were prepared and characterized (see Figure 2). As achiral cross-linking agents compounds **A**, **B**, and **C** were selected because

* To whom correspondence should be addressed. E-mail: bros@posta.unizar.es.

10.1021/ma001928e CCC: $20.00
Published on Web 05/11/2001

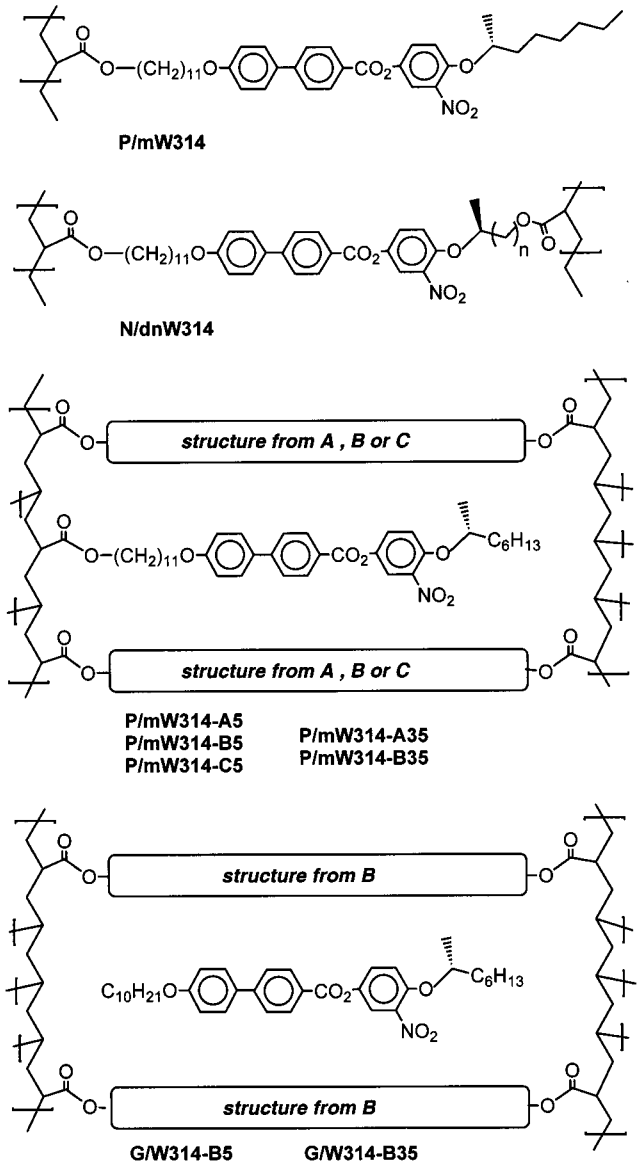

Figure 1. Structure of the polymeric materials obtained by in situ photopolymerization in the SmC* mesophase.

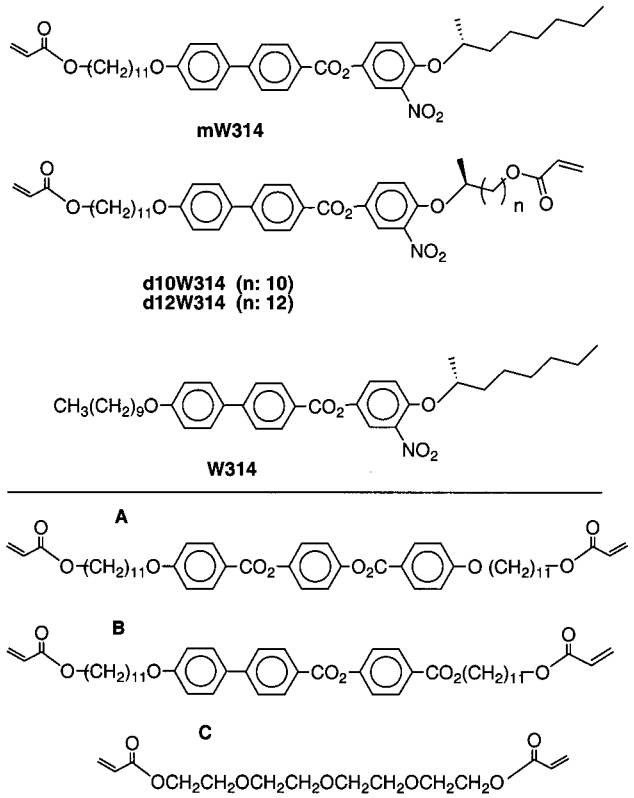

Figure 2. Structure of the low molecular weight compounds used to prepare the photopolymerizable samples.

they offer very different structural characteristics. While **C** is commercially available, **A** and **B** were synthesized and characterized in our laboratory.[12] For the sake of comparison, compound **W314** was also synthesized and characterized by us.

Results and Discussion

Monomers and Photopolymerizable Samples. A. Preparation of the Materials. To prepare the target polymeric materials, different low molar mass materials were prepared and characterized.

Three chiral reactive nitro compounds were synthesized. The monoreactive compound **mW314** that, after the polymerization process, would afford the side-chain polymer **P/mW314** or, when mixed with the achiral diacrylates **A**, **B**, and **C** in different proportions, would furnish the copolymers **P/mW314-A*n***, **P/mW314-B*n***, and **P/W314-C*n*** with different degrees of cross-linking (***n***, mol %). To prepare anisotropic networks, two chiral diacrylates **d10W314** and **d12W314** were prepared.

The synthetic pathway for compound **mW314** is shown in Scheme 1. A very similar synthetic strategy was followed to prepare the nonreactive compound **W314**. Compound **3** (Scheme 1) was prepared by nitration of 4-hydroxyphenylbenzoate using the conditions reported by Keller,[13] followed by the introduction of the chiral chain under Mitsunobu conditions and deprotection of the benzoate group. Esterification of phenol **3** with **7**, followed by a further dehydrohalogenation step, yielded compound **mW314**.

The preparation of the diacrylates **d10W314** and **d12W314** required the synthesis of the noncommercial chiral alcohols 13-tetradecen-2-ol (**10**) and 11-undecen-2-ol (**11**). Two different synthetic approaches were used in the preparation of the racemic compounds (Scheme 2). Compound (±)-**10** was obtained by using the method reported by Lub et al.,[14] although modification of the decarboxylation step was necessary.[15] Reaction of commercially available 10-undecenal with methylmagnesium iodide afforded compound (±)-**11** in one step. The racemic precursors were converted into the chiral compounds (−)-**10** and (−)-**11** by selective enzymatic acetylation catalyzed by pancreatic porcine lipase (PPL) and subsequent hydrolysis of the acetylated intermediate[16] (Scheme 2c). The *R* derivative was obtained for both compounds with 98% enantiomeric excess. The absolute configurations of the two alcohols were not established experimentally, but they were extrapolated from the results published by Wong et al.[16] for secondary alcohols. The synthesis of compounds **d10W314** and **d12W314** is outlined in Scheme 3.

Prior to the preparation of the polymeric materials, a study of the reactive binary mixtures was performed in order to select the most suitable systems for the photopolymerization in the polar liquid crystal phase. These samples were prepared by mixing in solution the appropriate proportions of the two components of the

Scheme 1. Synthesis of Monoacrylate mW314

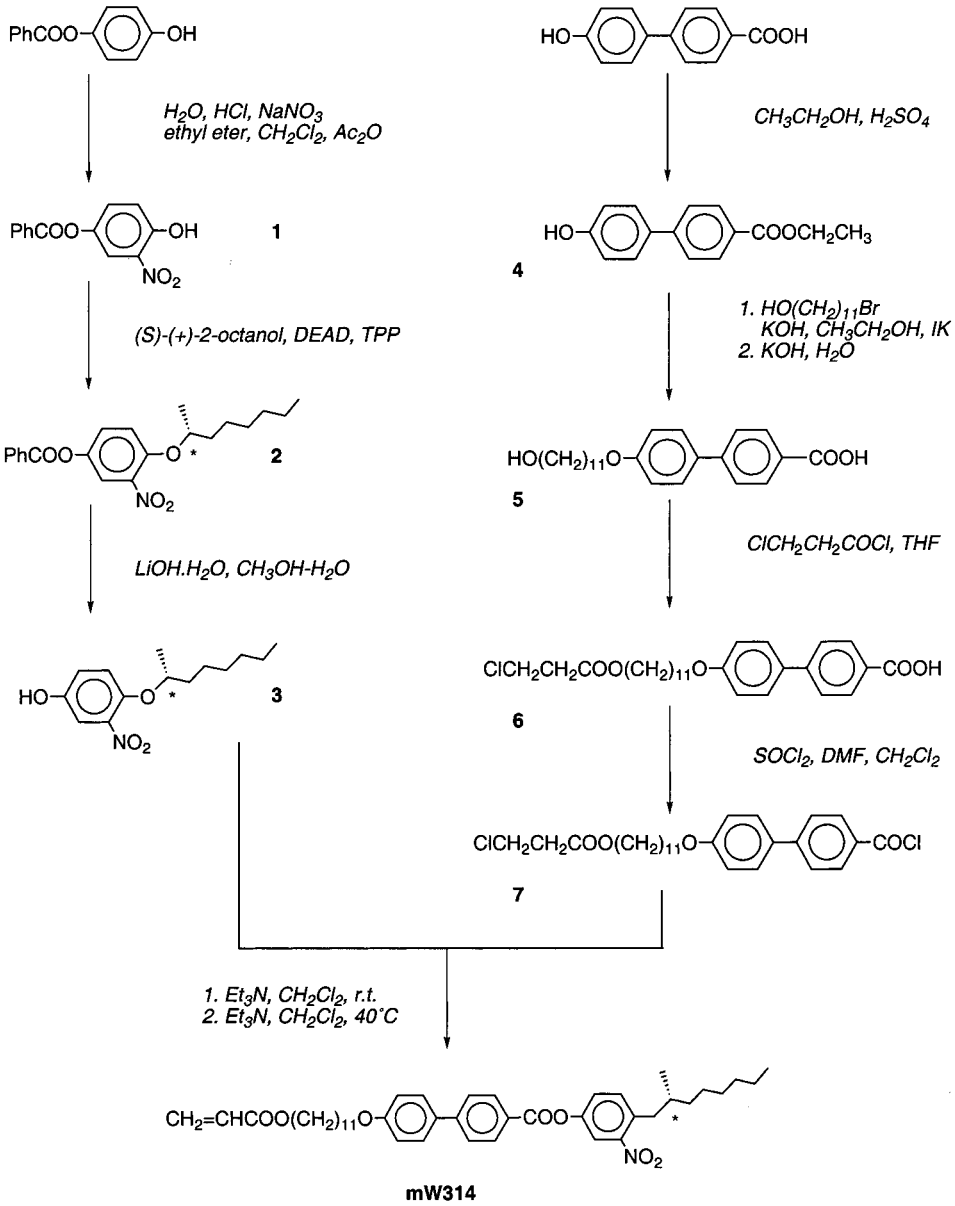

blend along with 200 ppm of 2,6-*tert*-butyl-4-methylphenol in order to avoid thermal polymerization during the characterization.

B. Liquid Crystal and Ferroelectric Properties of Materials. The mesomorphic behavior and transition temperatures of the monomers were studied by polarizing optical microscopy (OM) and differential scanning calorimetry (DSC). The results are collected in Table 1, which also includes the properties of **W314** as well as those of compounds **A** and **B**, which are used as cross-linkers. Compound **C** is not liquid crystalline and is a liquid at room temperature. To complete this table, synthetic intermediates **18**−**21**, which show liquid crystalline properties, are also considered.

All the nitro-derivatives exhibit both SmA and SmC* mesophases and, in most cases, the SmA−SmC* transition shows enthalpic changes. As can be seen, the incorporation of acrylate groups does not affect the phase sequences, but marked changes in transition temperatures are clear. On the other hand, if we compare compounds **d10W314** and **d12W314** with the octyloxy homologues (see Table 1, **d8W314**) previously reported by Trollsås et al.,[9] it can be seen out that long chiral terminal chains lead to the suppression of enantiotropic mesomorphism even though neither the type of mesophase nor the SmC* range are significantly modified.

Similar optical and calorimetric studies were performed with the photopolymerizable binary mixtures prepared. As a representative example, Figure 3 shows the liquid crystal phase diagrams for the different binary systems based on **mW314** and the cross-linkers **A** and **B**, which were used for the preparation of the copolymers **P/mW314-A*n*** and **P/mW314-B*n***.

All the mixtures studied show the required SmC* phase. The presence of greater than 50% of the cross-linking agent promotes the appearance of an N* phase or, in the case of cross-linker **A**, very short ranges of TGB phases or the presence of a SmX mesophase in some **mW314-B*n*** systems. These latter samples exhibit a dramatic texture change on entering from the SmC* (*schlieren* texture with two and four brushes), although this change is not evident by DSC. On the basis of the similar behavior detected for compound **B**,[17] we tenta-

Scheme 2. Synthesis of Chiral Secondary Alcohols (−)-10 and (−)-11

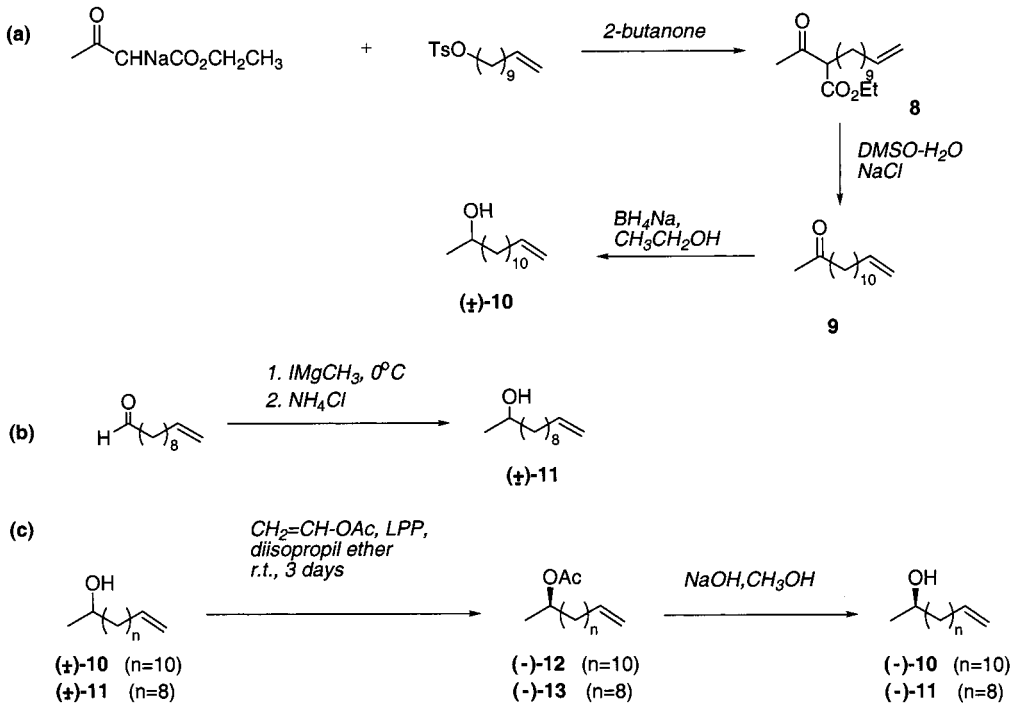

tively consider this mesophase to be SmC*$_{alt}$, although dielectric studies have not confirmed its antiferroelectric behavior.

Table 2 summarizes the liquid crystal properties of the binary mixtures chosen for the photopolymerization studies. These materials were selected on the basis that most of them present a SmC* phase, and in addition, they should provide different degrees of mobility in the final polymerized state. Mixtures **mW314-A5** and **mW314-B5** were taken as representative systems for a low degree of cross-linking, while systems with lower mobility but still with a significant amount of NLO-phore are represented by the 35 mol % homologues **mW314-A35** and **mW314-B35**. In the case of the cross-linker **C**, only the mixture **mW314-C5** was studied due to miscibility problems.

Precursors of the gels were analyzed in a similar way, but for comparative studies only binary mixtures with 5 and 35 mol % of the nonchiral diacrylate were fully characterized. These mixtures all exhibit a SmC* phase with the exception of **W314-A35**.

Table 3 shows the most relevant data (spontaneous polarization and tilt angle values) determined for the pure compounds and the ferroelectric photopolymerizable mixtures discussed above.

As can be seen, the pure nitro monomers show significant spontaneous polarization values in the SmC* phase, but in all cases they are lower than the P_s corresponding to the nonreactive parent compound **W314**. The lack of data in the literature cannot help to confirm the general drop in the polarization values upon introducing acrylates, but the outstanding dipolar coupling found for **W314** should also be considered.[3] As far as the binary blends are concerned, they behave as typical FLC materials in the sense that their P_s values gradually increase as the temperature decreases until saturation values are reached. On the other hand, the addition of achiral diacrylates clearly leads to polarizations lower than those of the pure nitro monomers, the decrease in P_s being faster than the linear function of the percentage of achiral component.

In Situ Photopolymerization of Samples. A. Study of the Photopolymerization Process. The reaction conditions for the preparation of all the polymeric materials were established by taking into account the following points:

1. UV−Vis characterization of the nitro monomers as well as the achiral diacrylates revealed that while the latter do not absorb above 350 nm, all the nitro compounds exhibit some absorption in the 350−400 nm region. Consequently, as the photopolymerization could be induced by a photoinitiator absorbing in the visible range, visible light was used. We initially considered different photoinitiators (Darocur 4265, Irgacure 369, Titanocene, and Lucirine TPO). The latter photoinitiator offered the best results.

2. The DSC technique was not appropriate to follow the progress of the polymerization process of any of the systems. Thus, the degree of conversion was evaluated through GPC analysis of the residual monomer of thin films polymerized under different experimental conditions.

3. Conversions higher than 84% and a M_w of around 89.000 (M_w/M_n:2.6) were determined for **P/mW314** prepared under the experimental conditions selected as standard: samples that contained 2 wt % of Lucirine TPO were irradiated for 5 min with an OSRAM Ultra-vitalux 300 W lamp placed at a distance of about 6 cm from the sample. Longer periods of time were needed for the preparation of anisotropic networks based on the nitrodiacrylates. The photopolymerization processes were carried out at a temperature of 30 °C in most cases.

These experimental conditions were applied to prepare both nonoriented thin films used for structural characterizations [GPC, OM, DSC, X-ray diffraction (XRD)] and aligned cells used for the SHG measurements and P_s studies (see Experimental Section).

The presence of gas bubbles in the gels with 5 mol % of network, as well as the crystallization of **d12W314**

Scheme 3. Synthesis of the Chiral Diacrylates d10W314 and d12W314.

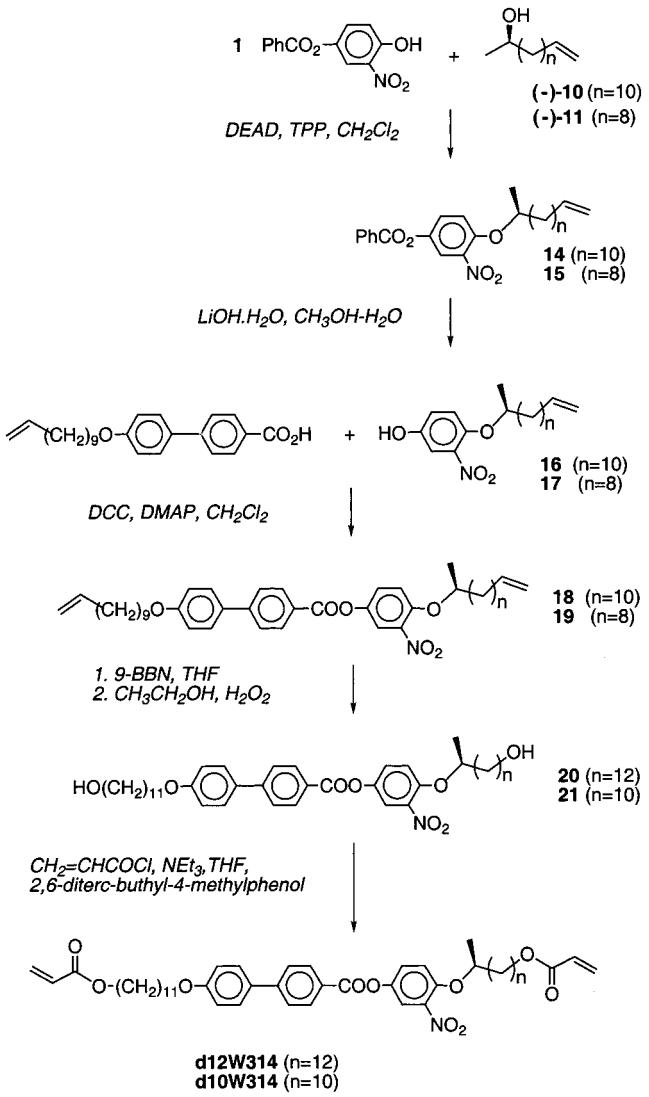

during the polymerization process, led us to discard the polymeric samples derived from these systems. However, the photopolymerization processes afforded good quality polymerized samples of the following materials: **P/mW314**, **P/mW314-A5**, **P/mW314-A35**, **P/mW314-B5**, **P/mW314-B35**, **P/mW314-C5**, **N/d10W314**, and **G/W314-B35**.

B. Mesogenic and Ferroelectric Characterization of the Photopolymerized Materials. The mesomorphic properties of the polymerized materials obtained by in situ photopolymerization in the SmC* phase are gathered in Table 4. These data were obtained using different techniques (DSC, OM, and XRD).

All the photopolymerized materials exhibit glass transitions (T_g) (except for gel **G/W314-B35**) as well as broad endothermic peaks at higher temperatures. The glass transition appears in a similar temperature range for **P/mW314** and the low cross-linking density copolymers (around 10 °C) and, as expected, increases for larger reticulated compounds. Surprisingly, in network **N/d10W314**, T_g was around 12 °C. **P/mW314** and the copolymer **P/mW314-C5** displayed similar behavior in the sense that their DSC traces show an overlap of both the melting peak and the glass transition. **G/W314-B35** showed very similar endotherms to pure **W314** but they were broader and occurred at slightly lower temperatures. This fact is attributed to the presence of two molecular populations due to the influence of the network walls.

OM revealed that gel **G/W314-B35** and materials with low percentages of cross-linker exhibit textures similar to those of the side-chain polymer **P/mW314**, and these were assigned as being due to SmC* and SmA mesophases. In the cases of materials with higher percentages of cross-linker, the textures of the monomeric samples are frozen by photopolymerization and a SmC* mesophase is obtained.

Macroscopic arrangement was confirmed by X-ray diffraction studies (Figure 4). Room-temperature X-ray diffraction patterns of films of **P/mW314** and the copolymers revealed two different layer thicknesses. One ranges from 36 to 45 Å depending on the material, i.e., on the nature of the cross-linking agent and on the degree of cross-linking. These reflections have been attributed to the presence of a monolayer structure that is consistent with the molecular length of **mW314** (46.5 Å from Dreiding models for a hypothetical all-anti conformation), and taking into account both the melting of the methylenic tails and the molecular tilt characteristic of a SmC* arrangement. Furthermore, a layer spacing of 37.5 Å was determined for the SmC* (at 49 °C) shown by **mW314**.

In addition to this, the X-ray patters yield another periodic distance, in the range 42−48 Å. These distances are not consistent with the monolayer spacing discussed above and there have been interpreted as being due to an interdigitated bilayer structure containing antiparallel NLO-phore units. As the degree of cross-linking increases, the interdigitated bilayer spacing becomes short-ranged, as revealed by the diffuse nature of the corresponding scattering maximum.

The coexistence of two types of molecular arrangement in the SmC*-like order of these materials is in good agreement with the observations reported elsewhere for some side-chain polymers.[18]

More complicated diffraction results were observed for **N/d10W314**. At room-temperature, many rings were found both at low and high angles, which can be accounted for by the coexistence of mesogenic-like order and a crystalline phase arising from the presence of residual diacrylate.[11]

All attempts to measure ferroelectric responses for these materials failed due to the high molecular weight, viscosity and structural mobility restrictions. Slight switching was detected for **P/mW314** by dielectric measurements, although this phenomenon could not be observed by OM.

Nonlinear Optical Properties. According to the C_2 symmetry that characterizes the SmC* phase, the second-order susceptibility tensor has the following form:

$$(\boldsymbol{d}_{ij}) = \begin{bmatrix} 0 & 0 & 0 & d_{25} & 0 & d_{21} \\ d_{21} & d_{22} & d_{23} & 0 & d_{25} & 0 \\ 0 & 0 & 0 & d_{23} & 0 & d_{25} \end{bmatrix} \qquad (1)$$

Here, Kleinman conditions are assumed to be valid. The tensor is referred to a coordinate system in which z is oriented along the optic axis and y is parallel to the spontaneous polarization, P_s.

When an NLO material is illuminated with linearly polarized light at frequency ω propagating along Z, the

Table 1. Phase Transition Temperatures of Monomers and Related Compounds

compound	phase transition temperature (°C) [kJ mol^{-1}][a,b]
W314	K 61.9 [44.2] SmC* 89.7 [0.2] SmA 115.3 [4.3] I
mW314	K 21.9 [19.9] SmC* 51.8 [0.3] SmA 64.5 [1.9] I
d8W314[9]	K 29 SmC* 33 SmA 39 I
	I 34 SmA 29 SmC* 8 K
d10W314	K 40.1 [43.0] I
	I 38.8 [1.2][c] N* 37.3[d] SmA 31.1 [0.3] SmC* 12.2 [29.1] K
d12W314	K 48.6 [61.4] I
	I 40.1 [1.6] SmA 36.9 [e]SmC* 21.6 [42.7] K
cross-linker **A**	K 73.4 [66.3] SmE 84.9 [5.5] SmC 115.8 [1.2] N 136.7 [2.1] I
cross-linker **B**	K 78.4 [63.5] SmC_{alt} 96.6[f] SmC 107.8 [0.1] SmA 117.3 [6.2] I
18	K 42.7 [41.4] SmC* 62.9 [0.4] SmA 93.6 [3.4] I
19	K 42.5 [38.8] SmC* 71.3 [0.1] SmA 95.7 [3.7] I
20	K 61.7 [44.1] SmC* 83.2 [0.3] SmA 101.4 [9.2] I
21	K 84.5 [47.1] SmC* 96.2 [0.1] SmA 111.0 [9.0] I

[a] K: crystalline phase. SmC*: chiral smectic C phase. SmA: smectic A phase. N*: chiral nematic phase. SmE: smectic E phase. SmC_{alt}: alternating smectic C phase. [b] Data determined by DSC, from second scans at a scanning rate of 10 °C/min. [c] Joined data from SmC*−SmA−I transition sequence. [d] Data corresponding to the maximum DSC peak. [e] Data determined by dielectric measurements. [f] Optical microscopic data.

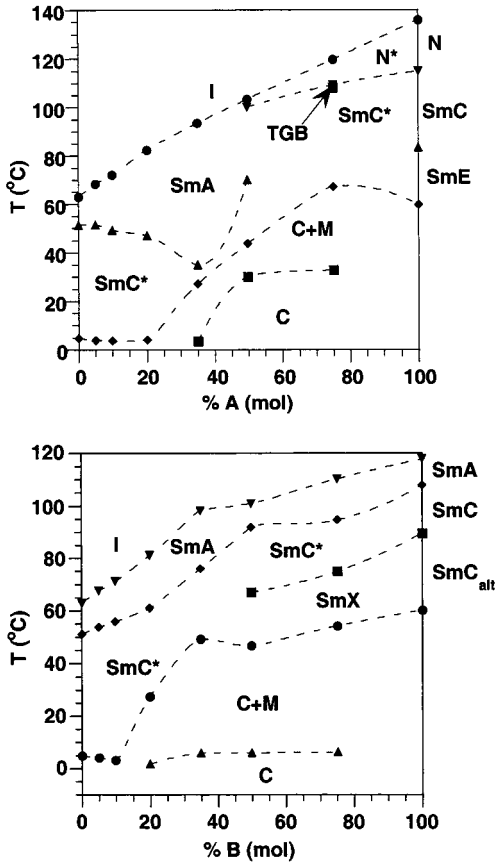

Figure 3. Phase diagrams obtained from the first cooling of the mixtures of **mW314** and the achiral diacrylates **A** (above) and **B** (below).

amplitude of the generated SH field can be expressed as

$$E_{\mathrm{I}}^{2\omega}(\mathrm{L}) = -i\omega\sqrt{\frac{\mu_0}{\epsilon}}\sum_{J,K} d_{IJK}E_J^{\omega}E_K^{\omega}\frac{e^{i\Delta k_{IJK}L}-1}{i\Delta k_{IJK}} \qquad I, J, K = X, Y \quad (2)$$

where X and Y are the directions of the eigenmodes of polarization in the crystal; L is the interaction length; $\Delta k_{IJK} = k_I^{2\omega} - (k_J^{\omega} + k_K^{\omega})$ is the phase mismatch, where $k_{J,K}^{\omega} = \omega n_{J,K}^{\omega}/c$ and $k_I^{2\omega} = 2\omega n_I^{2\omega}/c$ are the wave vectors corresponding to the fundamental and SH beams, respectively.

If we assume that materials behave as positive uniaxial media and show normal dispersion, then the ordinary and the extraordinary rays are along the Y and X directions, respectively. These rays propagate with refractive indices n_o and $n_e(\theta)$, where $n_e(\theta)$ is given by

$$\frac{1}{(n_e(\theta))^2} = \frac{\cos^2\theta}{n_o^2} + \frac{\sin^2\theta}{n_e^2} \quad (3)$$

Table 2. Transition Temperatures of the Photopolymerizable Samples Used in the Polymerization Experiments

sample	phase transition temperature (°C)[a,b]
W314-A5	I 110.2 SmA 82.9 SmC* 9.2 K
W314−B5	I 113.5 SmA 86.7 SmC* 12.4 K
W314-C5	I 106.7 SmA 73.6 SmC* 14.0 K
W314-A35	I 105.2 N* 103.0[c] SmA 5.5 K
W314-B35	I 106.6 SmA 74.5[c] SmC* 51.5[c] SmX 40.4 K
mW314-A5	I 68.3 SmA 51.4 SmC* 4.0 K
mW314-B5	I 67.6 SmA 53.8 SmC* 4.2 K
mW314-C5	I 57.6 SmA 43.8 SmC* 6.3 K
mW314-A35	I 93.5 SmA 35.0[d] SmC* 27.2 K
mW314-B35	I 90.1 SmA 76.0[c] SmC* 49.2 K

[a] K: crystalline phase. SmC*: chiral smectic C phase. SmA: smectic A phase. N*: chiral nematic phase. SmX: tentatively assigned as SmC^*_{alt}. [b] Data from the cooling processes determined by DSC (10 °C/min). [c] Optical microscopic data. [d] Data determined by dielectric measurements.

Table 3. Ferroelectric Properties of Pure and Photopolymerizable Samples

sample	$P_{s(max)}$ (nC cm^{-2})	P_s[a] (nC cm^{-2})	θ[a] (deg)	P_o[a,b]
W314	510	239	31	−464
mW314	259	164	28	−349
d10W314[c]	102	88	26	−201
d12W314[c]	46[d]	46[d]	16[d]	−167[d]
W314-A5	349	63	3	1203
W314-B5	359	89	4	1276
W314-C5	375	134	20	392
W314-A35	124	123		
W314-B35	103	60		
mW314-A5	134	101	22	270
mW314-B5	216	129	25	305
mW314-C5	186	141	28	300
mW314-A35	37	21		
mW314-B35	124	56		

[a] Data measured at $T_c - T = 10$ °C (T_c: SmA−SmC* phase transition temperature). [b] $P_o = P_s/\sin\theta$. [c] The sample did not show a perfect planar alignment. [d] Data measured at $T_c - T = 6$ °C.

Table 4. Transition Temperatures of the Polymeric Materials Obtained by in Situ Photopolymerization at the SmC* Phase

sample	phase transition temperature (°C)[a,b]
P/mW314	g 10 SmC* 94 SmA 143 I
P/mW314-A5	g 12 SmC* 90 [c]SmA 147 I
P/mW314-B5	g 11 SmC* 90[c] SmA 145 I
P/mW314-C5	g 9 SmC* 77 SmA 130 I
P/mW314-A35	g 36 SmC* [d]
P/mW314-B35	g 23 SmC* [d]
G/W314-B5[e]	K 60 SmC* 80 SmA 111 I
G/W314-B35	K 60 SmC*−SmA[c,f] 100 I
N/d10W314	g 12 SmC* [d]

[a] K: crystalline phase. SmC*: chiral smectic C phase. SmA: smectic A phase. g: glassy mesophase. [b] Data determined by DSC. T_g values were calculated as the inflection point in the baseline of the DSC thermogram (from second scannings at a rate of 20 °C/min). [c] Broad peak on DSC. [d] Isotropization transition is not observed. [e] All samples showed gas bubbles which made useless for SHG studies. [f] Sequence observed by optical microscopy.

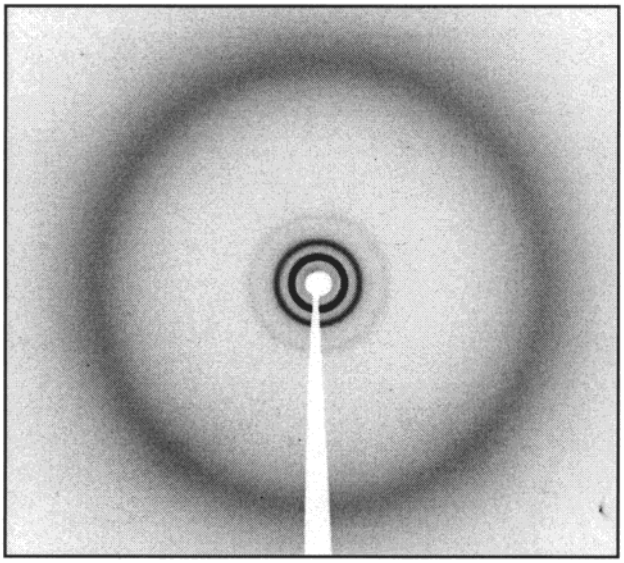

Figure 4. Room temperature X-ray diffraction patterns of thermally untreated raw polymer films of **P/mW314** (above) and **P/mW314-A35** (below).

n_o and n_e being the ordinary and extraordinary indices of the material.

In a general case the SHG signal is described by a very complex expression since it is obtained by squaring the field amplitude (eq 2), which in principle has the contribution of several terms.

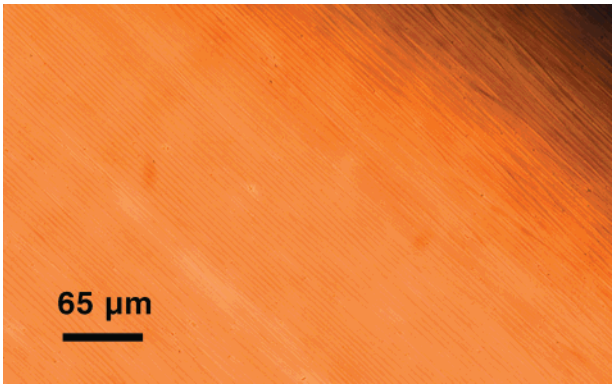

Figure 5. Polarized photomicrograph of the texture shown by **P/mW314-B5** at room temperature, in a 5 μm planar cell ($V_{dc} = 0$). This texture is representative of most of the polymerized materials.

Homeotropic cells are most commonly used in SHG investigations. However, we have shown that such cells are not practicable in the case of our FLC monomers. Electrohydrodynamic instabilities appear while applying electric fields due to the high amplitude necessary to unwind the helix characteristic of the SmC* phase. This phenomenon is presumably caused by the presence of large electric field gradients at the edges of the metallic spacers. For this reason, we restricted our study to thin planar cells, which do not present any problems with their alignments (see Figure 5).

Five different experimental configurations, which have already been introduced,[18] were used to obtain the complete ($\boldsymbol{d}_{ij}$) tensor together with the dispersion of the refractive indices and the birefringence at the fundamental frequency.

In the first two measurements (M1, M2) the cell is rotated around a vertical axis while the polarizer and analyzer are maintained horizontal. In M1 the director is set vertically (*oo-o* conversion) while it is set horizontally in M2 (*ee-e* conversion). It can be seen that a single term contributes to the SH signal under both conditions. In particular, the SH power can be expressed as a function of the angle of refraction θ_r and the dispersion $\Delta n_d = n_o^{2\omega} - n_o^{\omega}$ as

$$P^{2\omega}\left(\begin{Bmatrix} M1 \\ M2 \end{Bmatrix}\right) \propto \left(3\begin{Bmatrix} d_{21} \\ d_{23} \end{Bmatrix}\cos^2\theta_r \sin\theta_r + d_{22}\sin^3\theta_r\right)^2 \frac{\sin^2\left(\frac{2\pi}{\lambda}\Delta n_d L\right)}{\frac{2\pi}{\lambda}\Delta n_d} \quad (4)$$

On the other hand, in the cases of the other three configurations (M3−M5) the signal is measured as a function of the polarization angle of the incoming light. The cell is maintained fixed at an angle of incidence different from zero and oriented in such a way that the director is vertically (M3) or horizontally (M4, M5) arranged. In M3 and M4 the analyzer is fixed horizontally, whereas in M5 it is set vertically. In these three cases, since many material parameters are involved, $P^{2\omega}$ turns out to be a very complex expression sum of several terms. Thus, it is necessary to analyze the results through computer simulations because a simple fit to extract the unknown coefficients is not feasible.

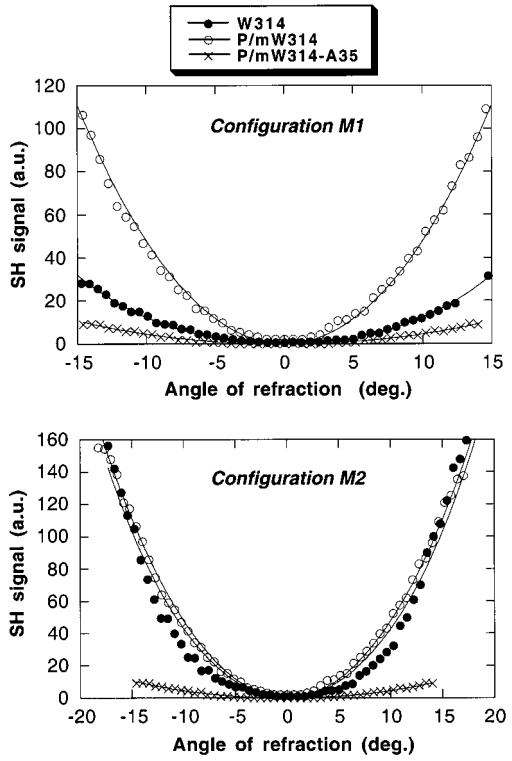

Figure 6. SH signal as a function of the angle of refraction and theoretical fits for some photopolymerized materials measured in the **M1** configuration (conversion *oo-o*) and the **M2** configuration (conversion *ee-e*), respectively.

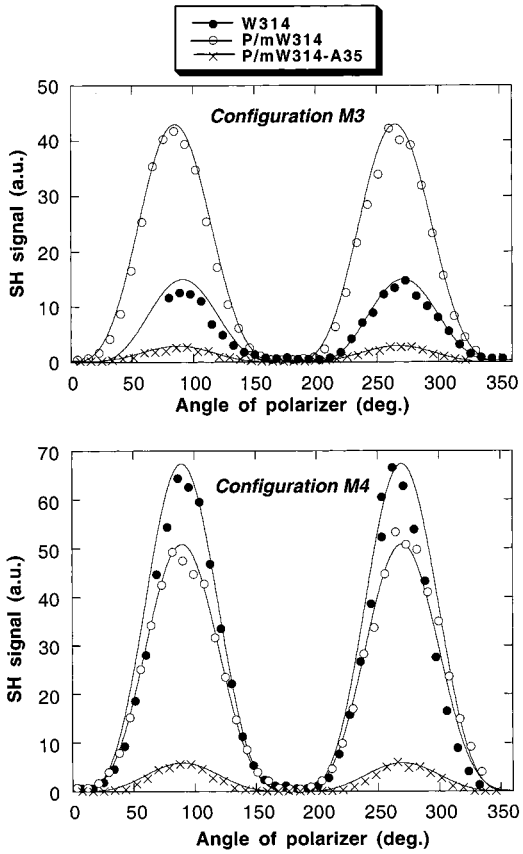

Figure 7. SH signal as a function of the polarizer angle for an angle of incidence of 20° and theoretical fits for some photopolymerized materials, measured in the **M3** and the **M4** configurations, respectively.

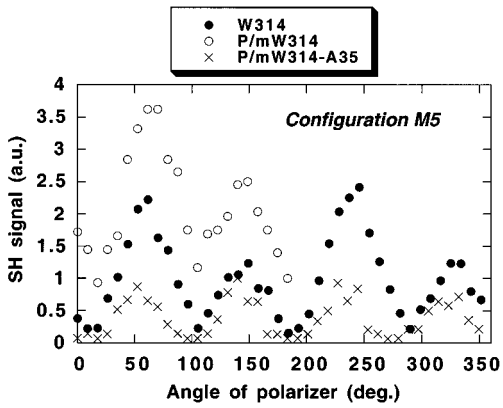

Figure 8. SHG for some photopolymerized materials measured in the **M5** configuration.

To extract the values corresponding to the individual parameters from the five configurations, we followed a method described in a previous study.[19]

Figures 6−8 show the experimental data for three representative materials (**W314**, **P/mW314**, and **P/mW314-35A**) together with the simulation profiles corresponding to each of the configurations described above.

After processing the five experimental profiles, we obtained the second-order susceptibility coefficients as well as the dispersion Δn_d and birefringence $\Delta n = n_e^{\omega} - n_o^{\omega}$. The results are presented in Table 5.

It can be seen that, in contrast to expectations, a substantial increase is not observed in SHG activity of the liquid crystalline materials after the polymerization process. In fact, the NLO coefficients corresponding to the side-chain polymer, which may be considered the most efficient material, are slightly higher than those corresponding to its low molecular weight counterpart. It is also evident that the SH efficiency decreases on diluting the NLO-phore by increasing the percentage of cross-linker. It is also clear from the results in Table 5 that the d_{22} coefficient is the highest coefficient for all the materials, which is not unexpected given that d_{22} is already substantially higher than the rest in the case of the low molecular weight compound **W314**. Nevertheless, one improvement that is worth pointing out is that most of these materials exhibit a polar structure at room temperature and without applying any electric field. This is a clear advantage in comparison with low molecular weight compounds. Despite the degree of cross-linking, gel **G/W314-35B** loses SHG activity on removing the applied electric field.

In 1996, Lim et al.[20] reported that the addition of an NLO-phore with high β_{zzz} to FLCs (i.e. 5% w/w of DANS) increases the SHG activity by as much as 10 to 1000 times, depending the particular d_{ij} coefficient. To investigate this possibility with our materials, we studied the efficiency of a mixture of **P/mW314** and the stilbene derivative **D**, namely **P/mW314-D5**, consisting of 5 mol % of dopant **D** and 95 mol % of **mW314**. This new material was prepared by in situ photopolymerization of the blend. This NLO-phore was previously studied in other materials and increased d_{33} up to 9 pm/V.[21] In addition, the viability of this material in photopolymerization processes is also documented.[22] However, data from this material (Table 5) show that this strategy did not provide any improvement with respect to the SmC* materials previously studied.

Table 5. d_{ij} Coefficients, Birefringence, and Dispersion for the Monomers and Polymeric Materials Studied (Uncertainties of the Data Were Estimated to Be Lower than 10%)

sample	d_{21} (pm/V)	d_{22} (pm/V)	d_{23} (pm/V)	d_{25} (pm/V)	Δn_d	Δn
W314[a]	0.060	0.30	0.120	−0.02	0.020	0.16
mW314[a]	0.062	0.30	0.095	−0.02	0.040	0.16
P/mW314[b]	0.080	0.35	0.095	−0.02	0.045	0.16
P/mW314-A5[b]	0.045	0.27	0.050		0.045	0.16
P/mW314-B5[b]	0.070	0.30	0.090		0.045	0.17
P/mW314-C5[b]	0.060	0.28	0.080	−0.05	0.045	0.16
P/mW314-A35[b]	0.028	0.15	0.042		0.050	0.17
P/mW314-B35[b]	0.040	0.15	0.048		0.055	0.18
N/d10W314[b]	0.040	0.30	0.060			
G/W314-B35[a]	0.032	0.10	0.034	−0.01	0.050	0.18
P/mW314-D5[b]	0.070	0.30	0.100	−0.04	0.040	0.16

[a] Data measured at 15 °C below the SmA−SmC* transition temperature and $V_{dc} \neq 0$ V. [b] Data measured at room temperature and $V_{dc} = 0$ V as raw samples after polymerization.

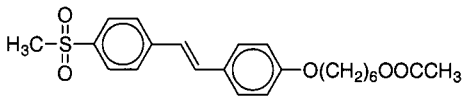

Figure 9. Structure of NLO-phore **D**, which was used as a dopant.

Summary

We have prepared and characterized a range of materials, obtained by in situ photopolymerization in the SmC* phase, to analyze the possibilities of this method for NLO purposes. Although the presence of a nitro group in the NLO-phore structure of these materials caused difficulties for both their polymerization and their study, the results obtained allow several important conclusions to be drawn:

•Most of the photopolymerized materials show SHG responses at room temperature without the application of electric fields, a fact that represents an advantage with respect to most of the low molecular mass FLCs reported to date.

•The SHG response increases slightly upon polymerization, but decreases with a decrease of the NLO-phore concentration.

•The side-chain polymer (**P/mW314**) and copolymers with low degrees of cross-linking are the most interesting materials. These systems combine the best NLO responses with a greater simplicity from the synthetic point of view.

Experimental Section

A. Synthesis of the Monomers. The synthetic pathways to obtain the monomers are shown in Schemes 1−3. Compound **C**, which was used as a cross-linker, was obtained from Aldrich. Organic starting chemicals were purchased from Aldrich or Lancaster and used as received. Lucirine TPO and NLO-phore **D** were kindly supplied by BASF and Philips, respectively.

Intermediates **1**−**4** have been previously reported in the literature,[8,9] and our characterizations match the data reported from them.

4′-(11″-Hydroxyundecyloxy)-4-biphenylcarboxylic Acid (5). A suspension of ethyl 4′-hydroxy-4-biphenylcarboxylate (5.00 g, 20.6 mmol), potassium hydroxide (1.33 g, 23.7 mmol), and potassium iodide (catalytic amount) in ethanol (20 mL) was stirred at room temperature for 1 h. 11-Bromo-1-undecanol (5.19 g, 20.6 mmol) was added, and the reaction mixture was refluxed for 24 h. A solution of potassium hydroxide (3.47 g, 61.9 mmol) in water (20 mL) was added. The reaction mixture was refluxed for 2 h and allowed to cool to room temperature. The precipitate was filtered off, poured into ethanol/water (30 mL), and acidified with concentrated HCl. The precipitate was collected by filtration and washed with hot acetonitrile. Yield: 6.4 g (75%). R_f (EtOAc−hexane 50%): 0.40. Mp: 201 °C. ^{1}H NMR (300 MHz, DMSO-d_6), δ: 1.20−1.40 (m, 16H), 1.60−1.80 (m, 2H), 3.33 (t, J = 6.6 Hz, 2H), 3.97 (t, J = 6.4 Hz, 2H), 7.00 (d, J = 8.8 Hz, 2H), 7.63 (d, J = 8.8 Hz, 2H), 7.70 (d, J = 8.4 Hz, 2H), 7.94 (d, J = 8.4 Hz, 2H). IR (NaCl), ν_{max}/cm^{-1}: 3500−2500, 1690, 1603, 1460.

4′-[11″-(3-Chloropropionyloxy)undecyloxy]-4-biphenylcarboxylic Acid (6). 3-Chloropropionyl chloride (1.19 g, 0.90 mL, 9.36 mmol) was added dropwise to a suspension of 4′-(11″-hydroxyundecyloxy)-4-biphenylcarboxylic acid (3.00 g, 7.8 mmol) in dry THF (20 mL) under nitrogen. The reaction mixture was refluxed for 2 h., allowed to cool to room temperature, and poured into a solution of concentrated HCl (9 drops) in ice (18 g) and water (70 mL) with vigorous stirring. The precipitate was filtered off, washed with water, and recrystallized from ethanol to give a white solid. Yield: 2.8 g (75%), R_f (EtOAc−hexane 4:1): 0.54. Mp: 154 °C. ^{1}H NMR (300 MHz, $CDCl_3$), δ: 1.15−1.55 (m, 14H), 1.55−1.75 (m, 2H), 1.75−1.90 (m, 2H), 2.77 (t, J = 6.7 Hz, 2H), 3.74 (t, J = 6.7 Hz, 2H), 3.99 (t, J = 6.5 Hz, 2H), 4.10 (t, J = 6.7 Hz, 2H), 6.97 (d, J = 8.7 Hz, 2H), 7.56 (d, J = 8.7 Hz, 2H), 7.64 (d, J = 8.3 Hz, 2H), 8.12 (d, J = 8.3 Hz, 2H). IR (NaCl), ν_{max}/cm^{-1}: 3500−3000, 1735, 1675, 1600, 1460.

(*R*)-4-(1′-Methylheptyloxy)-3-nitrophenyl 4′-Decyloxy-4-biphenylcarboxylate (W314). Pale yellow solid. Yield: 1.9 g (70%). R_f (CH_2Cl_2): 0.87. ^{1}H NMR (300 MHz, $CDCl_3$), δ: 0.87 (t, J = 6.5 Hz, 6H), 1.15−1.70 (m, 24H), 1.44 (d, J = 6.9 Hz, 3H), 1.72−1.88 (m, 2H), 4.00 (t, J = 6.6 Hz, t, 2H), 4.40−4.52 (m, 1H), 6.98 (d, J = 8.8 Hz, 2H), 7.09 (d, J = 9.1 Hz, 1H), 7.38 (dd, J = 9.1 Hz, 2.9 Hz, 1H), 7.58 (d, J = 8.8 Hz, 2H), 7.60−7.72 (m, 3H), 8.18 (d, J = 8.6 Hz, 2H). ^{13}C NMR (300 MHz, $CDCl_3$), δ: 164.8, 159.6, 149.5, 146.3, 142.8, 140.4, 131.7, 130.7, 128.3, 127.2, 126.6, 119.1, 116.4, 115.0, 36.2, 31.9, 31.7, 29.5, 29.4, 29.3, 29.2, 26.0, 25.2, 22.6, 22.5, 19.5, 14.1, 14.0. IR (NaCl), ν_{max}/cm^{-1}: 1738, 1533, 1464, 1259, 820, 762. MS FAB+, m/z (%): 170, 197, 223, 279, 337 (100%), 492. Anal. Calcd for $C_{37}H_{49}NO_6$: C, 73.60; H, 8.18; N, 2.32. Found: C, 73.53; H, 8.22; N, 2.40. $[\alpha]_D^{22}$ −29.8 (c = 1.042, $CHCl_3$).

(*R*)-4-(1′-Methylheptyloxy)-3-nitrophenyl 4′-(11″-Acryloyloxyundecyloxy)-4-biphenylcarboxylate (mW314). Thionyl chloride (0.60 mL, 0.90 g, 8.21 mmol) was added to a suspension of compound **6** (2.60 g, 5.47 mmol) and DMF (5 drops) in dry dichloromethane (8 mL) under nitrogen. The mixture was stirred at room temperature for 12 h. The solvent and the excess thionyl chloride were removed in vacuo. The solid obtained was dissolved in dry dichloromethane (65 mL) and added dropwise to a solution of (*R*)-4-(1′-methylheptyloxy)-3-nitrophenol (1.46 g, 5.47 mmol), triethylamine (0.99 mL, 0.72 g, 7.11 mmol) and 2,6-di-*tert*-butyl-4-methylphenol (catalytic amount) under nitrogen. The mixture was stirred at room temperature for 24 h under nitrogen. After this time, triethylamine (1.10 g, 1.52 mL, 10.94 mmol) was added and the mixture was refluxed for 8 h with protection from light. The reaction mixture was allowed to cool to room temperature, washed with water (×3) and dried ($MgSO_4$). The crude product was purified by column chromatography (silica gel, hexane/dichloromethane, 2:1) and recrystallized (twice) from ethanol to give a pale yellow solid. Yield: 2.9 g (78%). R_f (CH_2Cl_2): 0.69. ^{1}H NMR (300 MHz, $CDCl_3$), δ: 0.85−0.90 (m, 3H), 1.35 (d, J = 6.0 Hz, 3H), 1.25−1.85 (m, 28H), 4.00 (t, J = 6.6 Hz, 2H), 4.15 (t, J = 6.8 Hz, 2H), 4.45−4.55 (m, 1H), 5.80 (dd, J = 10.3, 1.5 Hz, 1H), 6.12 (dd, J = 17.3, 10.3 Hz, 1H), 6.40 (dd, J = 17.3, 1.5 Hz, 1H), 7.00 (d, J = 8.8 Hz, 2H), 7.10 (d, J = 9.3 Hz, 1H), 7.40 (dd, J = 9.3, 2.9 Hz, 1H), 7.60 (d, J = 8.8 Hz, 2H), 7.70 (d, J = 8.3 Hz, 2H), 7.72 (d, J = 2.9 Hz, 1H), 8.20 (d, J = 8.3 Hz, 2H). ^{13}C NMR (300 MHz, $CDCl_3$), δ: 166.3, 164.9, 159.7, 149.5, 146.4, 142.9, 140.4, 131.7, 130.8, 130.4, 128.6, 128.4, 127.3, 126.6, 119.1, 116.4, 115.0, 68.1, 64.7, 36.2, 31.7, 29.5, 29.4, 29.2, 29.1, 28.6, 26.0, 25.9, 25.2, 22.6, 22.6, 19.5, 14.0. IR (NaCl), ν_{max}/cm^{-1}: 2922, 2852, 1726, 1532, 1264, 1194, 1067, 826, 764. MS FAB+ m/z: 197, 223, 279, 349, 421. Anal.

Calcd for $C_{41}H_{53}NO_8$: C, 71.59; H, 7.77; N, 2.04. Found: C, 71.49; H, 7.88; N, 2.17. $[\alpha]_D^{22}$ −8.5 (c = 0.998, $CHCl_3$).

3-Carboxyethyl-13-tetradecen-2-one (8). A mixture of sodium acetylacetate (17.86 g, 117.4 mmol) and 10-undecenyl-4-toluenesulfonate (40 g, 123.3 mmol) in methyl ethyl ketone (300 mL) was refluxed for 24 h. The solvent was removed in vacuo, water (100 mL) was added, and the reaction mixture was extracted into diethyl ether (×3). The combined organic layers were washed with saturated $NaHCO_3$ and water and dried ($MgSO_4$). The solvent was removed in vacuo and the crude product purified by column chromatography (silica gel, hexane/ethyl acetate, 97:3). Colorless oil. Yield: 19.23 g (58%). R_f (CH_2Cl_2): 0.66. ^{1}H NMR (300 MHz, $CDCl_3$), δ: 1.20−1.40 (m, 19H), 1.95−2.05 (m, 2H), 2.19 (s, 3H), 3.36 (t, J = 7.3 Hz, 1H), 4.16 (q, J = 7.2 Hz, 2H), 4.88−5.02 (m, 2H), 5.72−5.88 (m, 1H). IR (film) ν_{max}/cm^{-1}: 1743, 1715, 1640, 1464,1357, 1241, 910.

13-tetradecen-2-one (9). NaCl (3.96 g, 67.81 mmol) was added to a solution of compound **8** (19.15 g, 67.81 mmol) in DMSO (50 mL) and water (3.5 mL). The reaction mixture was refluxed for 10 h and then allowed to cool to room temperature. Water (20 mL) was added and the mixture extracted into hexane (×3). The combined organic layers were washed with saturated NaCl (×3) and water and dried ($MgSO_4$). The solvent was removed in vacuo and the crude product purified by column chromatography (silica gel, hexane/ethyl acetate, 97:3) to give a colorless oil. Yield: 5.71 g (40%). R_f (CH_2Cl_2): 0.70. ^{1}H NMR (300 MHz, $CDCl_3$) δ: 1.10−1.60 (m, 16H), 1.95−2.05 (m, 2H), 2.1 (s, 3H), 2.39 (t, J = 7.4 Hz, 2H), 4.75−5.00 (m, 2H), 5.70−5.85 (m, 1H). IR (film), ν_{max}/cm^{-1}: 1715, 1463, 1359, 908.

(±)-13-tetradecen-2-ol ((±)-10). Sodium borohydride (193 mg, 5.10 mmol) was added slowly to a solution of **9** (3.90 g, 18.54 mmol) in ethanol (20 mL) in such a way that the temperature did not exceed 15 °C. The reaction mixture was stirred at room temperature for 2 h, and acetone (3 mL) was then added, followed by 10% aqueous NaOH (18 mL). The solvent was removed in vacuo, water was added, and the mixture was extracted into diethyl ether. The combined organic layers were washed with saturated NaCl and water and dried ($MgSO_4$). The solvent was removed in vacuo and the crude product purified by column chromatography (silica gel, dichloromethane) to give a colorless oil. Yield: 3.74 g (95%). R_f (CH_2Cl_2): 0.30. ^{1}H NMR (300 MHz, $CDCl_3$), δ: 1.14−1.50 (m, 18H), 1.18 (d, J = 6.8 Hz, 3H), 1.98−2.06 (m, 2H), 3.70−3.82 (m, 1H), 4.84−5.20 (m, 2H), 5.72−5.88 (m, 1H). IR (film) ν_{max}/cm^{-1}: 3350 (broad), 2927, 2855, 1641, 1464, 1374.

(±)-11-dodecen-2-ol ((±)-11). 10-Undecenal (20.25 g, 25 mL, 0.12 mol) was added dropwise to a 3 M solution of methylmagnesium iodide in dry diethyl ether (45 mL, 0.14 mol) at −10 °C under nitrogen. After 2 h of stirring at room temperature, saturated NH_4Cl was added (50 mL). The aqueous phase was extracted into diethyl ether (×2), and the combined organic phases were washed with water and dried ($MgSO_4$). The solvent was removed in vacuo and the crude product purified by column chromatography (silica gel, hexane to hexane/ethyl acetate, 85:15) to give a colorless oil. Yield: 19.91 g (80%). R_f (CH_2Cl_2): 0.30. ^{1}H NMR ($CDCl_3$). δ: 1.15 (d, J = 6.2 Hz, 3H), 1.20−1.50 (m, 14H), 1.98−2.06 (m, 2H), 3.70−3.82 (m, 1H), 4.84−5.20 (m, 2H), 5.72−5.88 (m, 1H). IR (film), ν_{max}/cm^{-1}: 3350 (broad), 2927, 2855, 1641, 1464, 1374.

2-Acetyloxy-13-tetradecene ((−)-12) and 2-Acetyloxy-11-dodecene ((−)-13). A mixture of racemic alcohol (±)-**10** or (±)-**11** (15.54 mmol), pancreatic porcine lipase (PPL) (2.02 g), and vinyl acetate (5.73 mL, 62.16 mmol) in dry diisopropyl ether (35 mL) was stirred for 3 d at room temperature. The mixture was filtered over Hyflo supercel, the solvent evaporated in vacuo, and the crude product purified by column chromatography (silica gel, hexane/dichloromethane, 3:1) to give a colorless oil. Yield: 29−31%. Gas chromatography (chiral column) showed an enantiomeric purity of 98%. Compound (−)-**12**. R_f (CH_2Cl_2): 0.63. ^{1}H NMR ($CDCl_3$). δ: 1.16 (d, J = 6.4 Hz, 3H), 1.20−1.50 (m, 18H), 1.98−2.06 (m, 5H), 4.80−5.00 (m, 3H), 5.72−5.88 (m, 1H). IR (film), ν_{max}/cm^{-1}: 1739, 1642, 1463, 1372, 1244, 1128, 1022, 953, 909. Compound (−)-**13**. R_f (CH_2Cl_2): 0.65. ^{1}H NMR ($CDCl_3$), δ: 1.16 (d, J = 6.4 Hz, 3H), 1.20−1.50 (m, 14H), 1.98−2.06 (m, 5H), 4.80−5.00 (m, 3H), 5.72−5.88 (m, 1H). IR (film), ν_{max}/cm^{-1}: 1740, 1642, 1463, 1372, 1245, 1128, 1022, 953, 910.

(−)-13-Tetradecen-2-ol ((−)-10) and (−)-11-dodecen-2-ol ((−)-11). A solution of compound (−)-**12** or (−)-**13** (7.53 mmol) and NaOH (9.03 mmol) in methanol (10 mL) was refluxed for 1 h. The reaction mixture was allowed to cool to room temperature and was neutralized with 2 M HCl. The solvent was removed in vacuo, water was added, and the mixture was extracted into diethyl ether (× 3). The combined organic phases were washed with saturated $NaHCO_3$ (× 3) and dried ($MgSO_4$). The solvent was removed in vacuo and the crude product purified by column chromatography (silica gel, dichloromethane) to give a colorless oil. Yield: 98%. ^{1}H NMR and IR data for (−)-**10** and (−)-**11** are the same as those given for (±)-**10** and (±)-**11**, respectively. (−)-**10**: $[\alpha]_D^{22}$ −5.83 (c = 0.120, $CHCl_3$). (−)-**11**: $[\alpha]_D^{22}$ −8.84 (c = 0.962, $CHCl_3$).

***(S)*-4-[2′-(13″-Tetradecenyloxy)]-3-nitrophenyl Benzoate (14) and *(S)*-4-[2′-(11″-Dodecenyloxy)]-3-nitrophenyl Benzoate (15).** Compounds **14** and **15** were prepared in a similar way to that described for the preparation of compound **2**. Both products were purified by column chromatography (silica gel, hexane/dichloromethane, 3:1). Compound **14**: yellow oil. Yield: 86%. R_f (CH_2Cl_2): 0.90. ^{1}H NMR ($CDCl_3$), δ: 1.20−1.50 (m, 16H), 1.35 (d, J = 6.1 Hz, 3H), 1.55−1.70 (m, 1H), 1.70−1.85 (m, 1H), 1.95−2.05 (m, 2H), 4.40−4.55 (m, 1H), 4.85−5.00 (m, 2H), 5.70−5.90 (m, 1H), 7.08 (d, J = 9.1 Hz, 1H), 7.37 (dd, J = 9.1 Hz, 2.9 Hz, 1H), 7.48−7.55 (m, 2H), 7.60−7.68 (m, 1H), 7.70 (d, J = 2.9 Hz, 1H), 8.17 (d, J = 7.2 Hz, 2H). IR (film), ν_{max}/cm^{-1}: 1742, 1530, 1353, 1246, 1196, 1057, 908, 815, 707. Compound **15**: yellow oil. Yield: 88%. R_f (CH_2Cl_2): 0.90. ^{1}H NMR ($CDCl_3$), δ: 1.20−1.50 (m, 12H), 1.35 (d, J = 6.1 Hz, 3H), 1.55−1.70 (m, 1H), 1.70−1.85 (m, 1H), 1.95−2.05 (m, 2H), 4.40−4.55 (m, 1H), 4.85−5.00 (m, 2H), 5.70−5.90 (m, 1H), 7.08 (d, J = 9.1 Hz, 1H), 7.37 (dd, J = 9.1 Hz, 2.9 Hz, 1H), 7.48−7.55 (m, 2H), 7.60−7.68 (m, 1H), 7.70 (d, J = 2.9 Hz, 1H), 8.17 (d, J = 7.2 Hz, 2H). IR (film), ν_{max}/cm^{-1}: 1741, 1531,1352, 1255, 1196, 1057, 908, 814, 706.

***(S)*-4-[2′-(13′-Tetradecenyloxy)]-3-nitrophenol (16) and *(S)*-4-[2′-(11′-Dodecenyloxy)]-3-nitrophenol (17).** Compounds **16** and **17** were prepared from compounds **14** and **15**, respectively, in a manner similar to that described for the preparation of compound **3**. The reaction mixture was cooled to 0 °C and acidified with concentrated HCl. The aqueous phase was extracted into diethyl ether (×3) and the combined organic phases washed successively with saturated $NaHCO_3$ (×3) and water and dried ($MgSO_4$). Compound **16**: yellow oil. Yield: 99%. R_f (CH_2Cl_2): 0.26. ^{1}H NMR ($CDCl_3$), δ: 1.20−1.45 (m, 19H), 1.50−1.65 (m, 1H), 1.65−1.80 (m, 1H), 1.95−2.05 (m, 2H), 4.25−4.40 (m, 1H), 5.00 (broad s, 1H), 4.85−5.00 (m, 2H), 5.70−5.85 (m, 1H), 6.90−7.00 (m, 2H), 7.26 (d, J = 2.9 Hz, 1H). IR (film), ν_{max}/cm^{-1}: 3500 (broad), 1529, 1442, 1349, 1265, 1218, 910, 815. Compound **17**: yellow oil. Yield: 98%. R_f (CH_2Cl_2): 0.26. ^{1}H NMR ($CDCl_3$), δ: 1.20−1.45 (m, 15H), 1.50−1.65 (m, 1H), 1.65−1.80 (m, 1H), 1.95−2.05 (m, 2H), 4.25−4.40 (m, 1H), 5.80 (broad, 1H), 4.85−5.00 (m, 2H), 5.70−5.85 (m, 1H), 6.90−7.00 (m, 2H), 7.26 (d, J = 2.9 Hz, 1H). IR (film), ν_{max}/cm^{-1}: 1527, 1348, 1263, 1217, 1149, 910, 737.

4″-[(*S*)-2-[(13-Tetradecenyl)oxy]-3-nitrophenyl 4-[4′-[(11-Undecenyloxy)phenyl]benzoate (18) and 4″-[(*S*)-2-[(11-Dodecenyl)oxy]-3-nitrophenyl 4-[4′-[(11-Undecenyloxy)phenyl]benzoate (19). *N*,*N*-Dicyclohexylcarbodiimide (2.31 g, 11.19 mmol) was added to a solution of the corresponding acid (8.61 mmol) and *N*,*N*-(dimethylamino)pyridine (0.158 g, 1.29 mmol) in dry dichloromethane (80 mL) at room temperature under nitrogen. The reaction mixture was stirred for 24 h at room temperature and then filtered through silica gel. The solvent was removed in vacuo, and the crude products were purified by column chromatography (silica gel, hexane/dichloromethane, 1:1) and recrystallized from ethanol. Compound **18**: pale yellow solid. Yield: 75%, R_f (CH_2Cl_2): 0.80. Mp: see Table 1. ^{1}H NMR ($CDCl_3$), δ: 1.20−1.70 (m, 29H), 1.35 (d, J = 6.0 Hz, 3H), 1.70−1.85 (m, 3H), 1.95−2.05 (m, 4H), 4.00 (d, J = 6.6 Hz, 2H), 4.45−4.55 (m, 1H), 5.05−5.85

(m, 4H), 5.75−5.85 (m, 2H), 6.98 (d, J = 8.6 Hz, 2H), 7.08 (d, J = 9.2 Hz, 1H), 7.38 (dd, J = 2.8 Hz, 9.2 Hz, 1H), 7.57 (d, J = 8.6 Hz, 2H), 7.68 (d, J = 8.3 Hz, 2H), 7.71 (d, J = 2.8 Hz, 1H), 8.18 (d, J = 8.3 Hz, 2H). ^{13}C NMR ($CDCl_3$), δ: 164.9, 159.9, 149.5, 146.6, 143.3, 140.9, 139.3, 139.2, 132.0, 130.8, 128.5, 127.1, 126.9, 126.7, 119.1, 116.8, 115.3, 114.2, 114.1, 68.4, 36.4, 33.8, 29.6, 29.56, 29.54, 29.5, 29.45, 29.4, 29.3, 29.2, 29.1, 29.02, 29.0, 26.1, 25.3, 19.6. IR (NaCl), ν_{max}/cm^{-1}: 1736, 1533, 1465, 1354, 1274, 910, 822, 764. MS EI m/z (%): 55, 69, 197, 349 (100%), 667, 697. Anal. Calcd for $C_{44}H_{59}NO_6$: C, 75.72; H, 8.52; N, 2.01. Found: C, 75.69; H, 8.43; N, 2.08. Compound **19**. Yield: 80%, Mp: see Table 1. R_f (CH_2Cl_2): 0.80. ^{1}H NMR ($CDCl_3$), δ: 1.20−1.70 (m, 25H), 1.35 (d, J = 6.0 Hz, 3H), 1.70−1.85 (m, 3H), 1.95−2.05 (m, 4H), 4.00 (d, J = 6.6 Hz, 2H), 4.45−4.55 (m, 1H), 5.05−5.85 (m, 4H), 5.75−5.85 (m, 2H), 6.98 (d, J = 8.6 Hz, 2H), 7.08 (d, J = 9.2 Hz, 1H), 7.38 (dd, J = 2.8 Hz, 9.2 Hz, 1H), 7.57 (d, J = 8.6 Hz, 2H), 7.68 (d, J = 8.3 Hz, 2H), 7.71 (d, J = 2.8 Hz, 1H), 8.18 (d, J = 8.3 Hz, 2H). ^{13}C NMR (300 MHz, $CDCl_3$), δ: 164.9, 159.7, 149.5, 146.4, 142.9, 140.5, 139.2, 139.1, 131.7, 130.8, 128.4, 127.3, 126.7, 119.1, 116.5, 115.0, 114.1, 68.1, 38.1, 36.2, 33.8, 29.5, 29.4, 29.2, 29.1, 28.9, 26.0, 25.3, 19.5. IR (NaCl) ν_{max}/cm^{-1}: 1736, 1531, 1464, 1352, 1274, 1149, 1064, 820, 762. MS FAB+ m/z: 349, 375, 401, 502, 531, 682. Anal. Calcd for $C_{42}H_{55}NO_6$: C, 75.30; H, 8.28; N, 2.10. Found: C, 75.39; H, 8.35; N, 2.02.

4″-((*S*)-2-((14-Hydroxy)dodecyl)oxy)-3-nitrophenyl 4-(4′-((11-Hydroxy)undecyl)oxy)phenylbenzoate (20) and 4″-((*S*)-2-((12-Hydroxy)dodecyl)oxy)-3-nitrophenyl 4-(4′-((11-Hydroxy)undecy)loxy)phenylbenzoate (21). A 0.5 M solution of 9-BBN in THF (16.0 mL, 8.00 mmol) was added over a period of 30 min to a solution of compound **18** or **19** (3.64 mmol) in 10 mL of dry THF at room temperature. After the mixture was stirred for 3 h, 5 mL of ethanol followed by 5 mL of 30% H_2O_2 was added. The resulting mixture was stirred for 1 h at room temperature, poured onto water, and extracted into dichloromethane (×3). The combined organic phases were washed with water and dried ($MgSO_4$). The solvent was evaporated in vacuo and the crude purified by column chromatography (silica gel, hexane to hexane/ethyl acetate, 95:5) and recrystallized from ethanol. Compound **20**: pale brown solid. Yield: 35−37%, Mp: see Table 1. ^{1}H NMR ($CDCl_3$), δ: 1.20−1.70 (m, 36H), 1.35 (d, J = 6.0 Hz, 3H), 1.70−1.85 (m, 4H), 3.62 (t, J = 6.4 Hz, 4H), 4.00 (t, J = 6.6 Hz, 2H), 4.45−4.55 (m, 1H), 6.98 (d, J = 8.6 Hz, 2H), 7.08 (d, J = 9.2 Hz, 1H), 7.38 (dd, J = 2.8 Hz, 9.2 Hz, 1H), 7.57 (d, J = 8.6 Hz, 2H), 7.68 (d, J = 8.3 Hz, 2H), 7.71 (d, J = 2.8 Hz, 1H), 8.18 (d, J = 8.3 Hz, 2H). IR (NaCl), ν_{max}/cm^{-1}: 3400−3200, 1736, 1533, 1462, 1377, 1267, 1066, 1036, 825, 723. Anal. Calcd for $C_{44}H_{63}NO_8$: C, 72.00; H, 8.65; N, 1.91. Found: C, 72.15; H, 8.50; N, 2.02. Compound **21**: pale brown solid. Yield: 35%, Mp: see Table 1. ^{1}H NMR ($CDCl_3$), δ: 1.20−1.70 (m, 32H), 1.35 (d, J = 6.0 Hz, 3H), 1.70−1.85 (m, 4H), 3.62 (t, J = 6.4 Hz, 4H), 4.00 (t, J = 6.6 Hz, 2H), 4.45−4.55 (m, 1H), 6.98 (d, J = 8.6 Hz, 2H), 7.08 (d, J = 9.2 Hz, 1H), 7.38 (dd, J = 2.8 Hz, 9.2 Hz, 1H), 7.57 (d, J = 8.6 Hz, 2H), 7.68 (d, J = 8.3 Hz, 2H), 7.71 (d, J = 2.8 Hz, 1H), 8.18 (d, J = 8.3 Hz, 2H). IR (NaCl), ν_{max}/cm^{-1}: 3400−3200, 1736, 1533, 1462, 1377, 1267, 1066, 1036, 825, 723. Anal. Calcd for $C_{42}H_{59}NO_8$: C, 71.46; H, 8.42; N, 1.98. Found: C, 71.58; H, 8.43; N, 2.02.

4″-((*S*)−(+)-2-((14-Acryloyloxy)tetradecyl)oxy)-3-nitrophenyl 4-{4′-((11-Acryloyloxy)undecyl)oxy)phenylbenzoate (d12W314) and 4″-((*S*)−(+)-2-((12-Acryloyloxy)dodecyl)oxy)-3-nitrophenyl 4-{4′-((11-Acryloyloxy)undecyl)-oxy)phenylbenzoate (d10W314). Freshly distilled acryloyl chloride (3.48 mmol) dissolved in dry THF (10 mL) was added dropwise to a solution of diol (1.34 mmol), triethylamine (4.02 mmol), and 2,6-di-*tert*-butyl-4-methylphenol (catalytic amount) in dry THF (10 mL) at 0 °C under nitrogen. The reaction mixture was stirred for 24 h at room temperature and poured into a 15% aqueous solution of NH_4Cl. The aqueous phase was extracted into dichloromethane (×3) and the combined organic layers were washed with water and dried ($MgSO_4$). The solvent was evaporated in vacuo and the crude product purified by column chromatography (silica gel, hexane to hexane/ethyl acetate, 4:1) and recrystallized from ethanol. Compound **d12W314**: pale yellow solid. Yield: 60%. R_f (CH_2Cl_2): 0.70. ^{1}H NMR ($CDCl_3$), δ: 1.15−1.50 (m, 28H), 1.35 (d, J = 6.0 Hz, 3H), 1.55−1.70 (m, 8H), 1.70−1.85 (m, 4H), 4.00 (t, J = 6.6 Hz, 2H), 4.13 (t, J = 6.8 Hz, 4H), 4.45−4.55 (m, 1H), 5.79 (dd, J = 10.4, 1.5 Hz, 2H), 6.10 (dd, J = 17.3, 10.4 Hz, 2H), 6.38 (dd, J = 17.3, 1.5 Hz, 2H), 6.99 (d, J = 8.8 Hz, 2H), 7.09 (d, J = 9.1 Hz, 1H), 7.38 (dd, J = 9.1, J = 2.9 Hz, 1H), 7.58 (d, J = 8.8 Hz, 2H), 7.68 (d, J = 8.7 Hz, 2H), 7.71 (d, J = 2.9 Hz, 1H), 8.18 (d, J = 8.7 Hz, 2H). ^{13}C NMR ($CDCl_3$), δ: 166.4, 164.9, 159.7, 149.5, 146.4, 142.9, 140.5, 131.8, 130.4, 128.6, 127.3, 126.7, 119.1, 116.5, 115.0, 68.1, 64.7, 38.7, 38.1, 36.2, 29.5, 29.3, 29.2, 28.6, 26.0, 25.2, 19.5. IR (NaCl), ν_{max}/cm^{-1}: 1726, 1537, 1460, 1269, 1198, 987, 814. MS FAB+ m/z (%): 349, 365, 421 (100%), 647, 663, 685, 864. Anal. Calcd for $C_{50}H_{67}NO_{10}$: C, 71.32; H, 8.02; N, 1.66. Found: C, 71.30; H, 7.99; N, 1.68. $[\alpha]_D^{22}$ +7.5 (c = 0.770, $CHCl_3$). Compound **d10W314**: pale yellow solid. Yield: 62%. R_f (CH_2Cl_2): 0.70. ^{1}H NMR (300 MHz, $CDCl_3$), δ: 1.20−1.50 (m, 24H), 1.35 (d, J = 6.0 Hz, 3H), 1.55−1.70 (m, 8H), 1.70−1.85 (m, 4H), 4.00 (t, J = 6.6 Hz, 2H), 4.13 (t, J = 6.8 Hz, 4H), 4.45−4.55 (m, 1H), 5.79 (dd, J = 10.4, J = 1.5 Hz, 2H), 6.10 (dd, J = 17.3, 10.4 Hz, 2H), 6.38 (dd, J = 17.3, J = 1.5 Hz, 2H), 6.99 (d, J = 8.8 Hz, 2H), 7.09 (d, J = 9.1 Hz, 1H), 7.38 (dd, J = 9.1, 2.9 Hz, 1H), 7.58 (d, J = 8.8 Hz, 2H), 7.68 (d, J = 8.7 Hz, 2H), 7.71 (d, J = 2.9 Hz, 1H), 8.18 (d, J = 8.7 Hz, 2H). ^{13}C NMR (300 MHz, $CDCl_3$), δ: 166.3, 164.9, 159.7, 149.5, 146.4, 142.9, 140.5, 131.8, 130.8, 130.4, 128.6, 128.4, 127.3, 126.7, 119.1, 116.4, 115.0, 68.1, 64.7, 64.6, 36.2, 29.5, 29.4, 29.3, 29.2, 28.6, 26.0, 25.9, 25.2, 19.5. IR (NaCl), ν_{max}/cm^{-1}: 1722, 1537, 1462, 1269, 1198, 982, 809. MS FAB+ m/z (%): 349, 367, 421 (100), 647, 662, 685, 836. Anal. Calcd for $C_{48}H_{63}NO_{10}$: C, 70.82; H, 7.80; N, 1.72. Found: C, 70.95; H, 7.77; N, 1.69. $[\alpha]_D^{22}$ +7.8 (c = 0.890, $CHCl_3$).

B. In Situ Photopolymerization. The photopolymerizable samples were prepared by dissolving the appropriate proportions of the different monomers, 2% (by weight) of the photoinitiator and 200 ppm of 2,6-di-*tert*-butyl-4-methylphenol (thermal inhibitor) in freshly distilled dichloromethane. The solvent was evaporated at room temperature and the residual solvent was removed by heating the sample at 30 °C under vacuum overnight.

Photopolymerization was studied by the analysis of the residual monomers by GPC. Standard photopolymerization conditions were as follows: 2% (w/w) of LUCIRINE TPO and an OSRAM Ultravitalux 300 W lamp. The sample was heated slightly above the isotropization temperature and cooled to the required temperature (SmC* phase). After stabilization for 5 min at this temperature, the lamp was placed at a distance of about 6 cm from the cell or aluminum pans. The irradiation was maintained for 5 min at isothermal conditions at the selected polymerization temperature. To prepare tridimensional networks (**N**) longer periods of time were needed (10−20 min). An IR filter was placed between the lamp and the samples to prevent the heating of the material during the photopolymerization process.

C. Experimental Details of the Ferroelectric Measurements. The spontaneous polarization values (P_s) were determined by integrating the displacement current peak, which appears due to the reversal of P_s, as a response to an applied triangular voltage.[23] Polyimide-coated unidirectional rubbed cells (from LINKAM) of 5 and 7.5 μm thickness and planar configuration were used. The maximum amplitude and frequency applied for the monomers was 40 Vpp and 50 Hz, respectively. Except for the diacrylates, good alignment was obtained by slowly cooling (0.5 or 1 °C/min) the filled cell from the isotropic to the SmA phase. The sign of the P_s was determined by the field reversal method through optical observation of the extinction direction by rotating the stage according to Lagerwall's convention.[24] The tilt angles were measured as a function of temperature, as half the rotation angle between the two extinction positions. To avoid an undesired photopolymerization, the materials were illuminated with red light during the sample preparation procedure.

D. Experimental Details of the NLO Measurements. Sample Preparation. Commercial planar cells (EHC) of a nominal thickness of 2 μm were chosen for our SHG measure-

ments. The real thickness of each cell (2−3 μm) was determined by means of an interferometric technique.

The liquid crystalline material was introduced into the cell in the isotropic phase. The cell was inserted into a temperature-controlled stage with optical access. Good alignment of the smectic layers was obtained in the SmC* phase by slow cooling under a square wave electric field of 10 V/μm and 5 Hz. We observed by polarizing optical microscopy that a dc voltage of 30 V was sufficient to unwind the helix at room temperature for all the materials studied.

The photopolymerization was carried out in all cases under a dc voltage of 30 V and at a temperature of 30 °C (in most cases). After this stage, the polymerized materials did not exhibit any ferroelectric switching under OM.

SHG Experimental Setup. A standard technique was used in our SHG measurements. The fundamental light came from a Q-switched Nd:YAG laser (wavelength $\lambda = 1064$ nm, pulse width = 6 ns, and repetition rate = 5 pulses/s) with a 10 MW/cm^2 intensity peak at the sample position. A beam splitter diverted a small part of the fundamental beam to a reference branch in which a crystal of $LiNbO_3$ was located. The second harmonic intensities were detected by two photomultipliers after passing an IR cut filter, a green glass filter, and an interference filter. The SH signal from the sample was divided by the one from the reference branch in order to compensate for the laser pulse spreading and intensity fluctuations. A y-cut quartz sample ($d_{11} = 0.4$ pm/V) was used as a standard for calibration purposes.

E. Techniques. Optical absorption measurements were taken using an ATI Unicam UV4 spectrophotometer. Infrared spectra for all the compounds were obtained using a Perkin-Elmer 1600 (FTIR) spectrophotometer in the 400−4000 cm^{-1} spectral range. ^{1}H and ^{13}C NMR spectra were recorded on a Varian Unity 300 MHz spectrometer and Bruker ARX-300-MHz spectrometer with samples in solution. Microanalysis was performed with a Perkin-Elmer 2400 microanalyzer. Mass spectrometry studies (EI and FAB+) were performed with a VG AutoSpec EBE spectrometer. Gas chromatography (HP 5890 Series II) with a Cyclodexb 112−2532 column was used for enantiomeric excess determinations. Specific rotations were measured using a Perkin-Elmer 241-AC polarimeter on either neat samples or solutions. Gel permeation chromatography (GPC) was carried out using a Waters HPLC set up equipped with a 600E multisolvent delivery system and a 996 photodiode array detector. Two Ultrastyragel columns (Waters) of 500 and 10^4 Å pore sizes were connected in series using THF as the mobile phase (0.8 mL/min) and polystyrene as calibration standard.

Mesomorphic properties were studied by OM using an Olympus BH2 microscope and a Linkam THMS 600 hot-stage. Transition temperatures were determined by differential scanning calorimetry (DSC) using either a TA2910 differential calorimeter or Perkin-Elmer DSC-7. These systems were calibrated with indium (156.6 °C, 28.44 J/g) and tin (232.1 °C, 60.5 J/g) using a scanning rate of 10 °C/min. X-ray diffraction patterns were obtained with an evacuated pinhole camera (Anton-Paar) operating with a point-focused Ni-filtered Cu Kα beam. For the polymeric materials, free films were obtained by photopolymerization of a molten sample between two untreated glass slides The samples were held in Lindemann glass capillaries (1 mm diameter) and heated, when necessary, with a variable-temperature attachment. The diffraction patterns were collected on flat photographic films.

Polarization and tilt angle studies were carried out using commercial cells with ITO electrodes coated with polyimide. The triangular wave voltage was supplied by an HP3325A function generator; the current−voltage cycles were recorded by an HP7090A digital acquisition system. All the equipment was interfaced to a microcomputer. The switching of the samples was studied by means of a photomultiplier hooked-up to the microscope (Nikon). The signal was registered in an oscilloscope (Tektronix TDS 310). The square wave voltage was supplied by an HP3245A function generator.

Acknowledgment. C.A. and N.P.) thank the Spanish Comisión Interministerial de Ciencia y Tecnología (CICYT) for their grants. This work was financially supported by the CICYT, Projects No. MAT97-0986-C02 and MAT99-1009-C02, and by the Universidad del Pais Vasco, Project No. 063.310-EB158/97. The authors gratefully acknowledge Dr. J. Barberá for the X-ray measurements and Dr. J. Lub from Philips for the supply of compound **D**, and we also acknowledge BASF for kindly supplying the photoinitiator LUCIRINE TPO.

References and Notes

(1) Prasad, P. N.; Williams, D. J. *Introduction to Nonlinear Optical Effects in Molecules and Polymers*; Wiley: New York. 1991.

(2) *Nonlinear Optical Properties of Organic Molecules and Crystals*; Chelma, D. S., Zyss, J., Eds.; Academic: London. 1987.

(3) Walba, D. M.; Ros, M. B.; Clark, N. A.; Shao, R.; Robinson, M. G.; Liu, J. Y.; Johnson, K. M.; Doroski, D. J. *J. Am. Chem. Soc.* **1991**, *113*, 5472.

(4) Schmidt, K.; Her, R. P.; Schadt, M.; Fünfschilling, J.; Buchecker, R.; Chien, X. H.; Benecke, C. *Liq. Cryst.* **1993**, *14*, 1735.

(5) Walba, D. M.; Dyer, D. J.; Cobben, P. L.; Sierra, T.; Rego, J. A.; Liberko, C. A.; Shao, R.; Clark, N. A. *Ferroelectrics* **1996**, *179*, 211.

(6) Espinet, P.; Etxebarria, J.; Folcia, C. L.; Ortega, J.; Ros, M. B.; Serrano, J. L. *Adv. Mater.* **1996**, *8*, 745.

(7) Walba, D. M.; Wand, M. D.; Thurmes, W. N. *Polym. Prepr. (Am. Chem. Soc., Div. Polym. Chem.)* **1993**, *34*, 697.

(8) (a) Trollsås, M.; Sahlén, F.; Gedde, U. W.; Hult, A.; Hermann, D.; Rudquist, P.; Komitov, L.; Lagerwall, S. T.; Stebler, B.; Lindström, J.; Rydlund, O. *Macromolecules* **1996**, *29*, 2590. (b) Sahlén, F.; Trollsås, M.; Hult, A.; Gedde, U. W. *Chem. Mater.* **1996**, *8*, 382.

(9) Trollsås, M.; Orrenius, C.; Sahlén, F.; Gedde, U. W.; Torbjörn, N.; Hult, A.; Hermann, D.; Rudquist, P.; Komitov, L.; Lagerwall, S. T.; Lindström, J. *J. Am. Chem. Soc.* **1996**, *118*, 8542.

(10) Hermann, D.; Rudquist, P.; Lagerwall, S. T.; Komitov, L.; Stebler, B.; Lindgren, M.; Trollsås, M.; Sahlén, F.; Hult, A.; Gedde, U. W.; Orrenius, C.; Norin, T. *Liq. Cryst.* **1998**, *24*, 295.

(11) Pereda, N.; Etxebarria, J.; Folcia, C. L.; Ortega, J.; Artal, C.; Ros, M. B.; Serrano, J. L. *J. Appl. Phys.* **2000**, *87*, 217.

(12) Pereda, N.; Etxebarria, J.; Folcia, C. L.; Ortega, J.; Artal, C.; Ros, M. B.; Serrano, J. L. Presented at the 17th International Liquid Crystal Conference, Strasbourg, France, 1998; Poster 2−56.

(13) Keller, P. *Bull. Soc. Chim. Fr.* **1994**, *131*, 27.

(14) Lub, J.; Van der Veen, J. H.; Van Echten, E. *Mol. Cryst. Liq. Cryst.* **1996**, *1287*, 205.

(15) (a) Krapcho, A. P. *Synthesis* **1982**, 805. (b) Krapcho, A. P. *Synthesis* **1982**, 893.

(16) Wand, Y.; Lalonde, M.; Momongan, M.; Bergbreiter, D. E.; Wong, C. *J. Am. Chem. Soc.* **1988**, *110*, 7200.

(17) De la Fuente, R.; Martin, E.; Pérez-Jubindo, M. A.; Artal, C.; Ros, M. B.; Serrano, J. L. *Liq. Cryst.* **2001**, *28*, 151.

(18) Omenat, A.; Hikmet, R. A. M.; Lub, J.; van der Sluis, P. *Macromolecules* **1996**, *29*, 6730.

(19) Pereda, N.; Folcia, C. L.; Etxebarria, J.; Ortega, J. *Liq. Cryst.* **1998**, *26*, 375.

(20) Lim, M.; Park, B.; Eom, S. Y.; Lee, S. D. *Mol. Cryst. Liq. Cryst.* **1996**, *280*, 59.

(21) Rikken, G. L. J. A.; Seppen, C. J. C.; Nijhuis, S.; Meijer, E. W. *Appl. Phys. Lett.* **1991**, *58*, 435.

(22) Broer, D. J.; Lub, J.; Mol, G. N. *Nature* **1995**, *378*, 467.

(23) De la Fuente, M. R.; Ezcurra, A.; Pérez-Jubindo, M. A.; Zubia, J. *Liq. Cryst.* **1990**, *7*, 51.

(24) Lagerwall, S. T.; Dahl, I. *Mol. Cryst. Liq. Cryst.* **1984**, *114*, 151.

MA001928E